Propagating and Scattering of the Electromagnetic Vortex Generated by a Spiral Parabolic Antenna

B. H. Yin, Z. He, and R. S. Chen

Department of Communication Engineering
Nanjing University of Science and Technology, Nanjing, 210094, China
eerschen@mail.njust.edu.cn

Abstract ─ A modified octree grouping scheme of the multilevel fast multipole algorithm (MLFMA) is proposed to analyze the electromagnetic (EM) scattering from the electrically large target, which is illuminated by a spiral parabolic antenna. The spiral parabolic antenna is used to generate the electromagnetic vortex of a specific mode number by adjusting the height of split. The proposed method builds two octree groups and decouples the interaction between the antenna and the target, so as to save the computational resource and improve the computational efficiency. Using this scheme, the numerical example with double metal spheres illuminated by the electromagnetic vortex reveals some special phenomena due to the spiral phase distribution, while the example with a scaled-down airplane at long operating range demonstrates that the electromagnetic vortex tends to be plane wave locally with the increase of propagation distance.

Index Terms ─ Electromagnetic vortex, incorporate modeling, MLFMA, octree grouping, orbital angular momentum, spiral parabolic antenna.

I. INTRODUCTION

Orbital angular momentum (OAM) has been found in the laser of the Laguerre-Gaussian mode for a few decades [1]. The electromagnetic wave carrying orbital angular momentum is also called the electromagnetic vortex or the vortex electromagnetic beam. The orbital angular momentum number carried by the electromagnetic vortex is defined as the topological charge or the mode number l. A large quantity of research has been conducted in optics so far, such as the micro-particle operation [2], the optical communication [3], the rotating objects detection [4], etc. The investigation of OAM in the radio domain falls behind optics. In 2007, Thidé proposed a generation method of the vortex electromagnetic beam in the low-frequency radio domain [5]. Since then, a series of explorations on the OAM-based communication and detection have springed up like mushrooms. Tamburini and Thidé conducted a series of wireless communication experiments on the

electromagnetic vortex, which validate the feasibility of the multiplexing scheme using orbital angular momentum [6-8]. However, some scholars put forward their doubts and considered that the OAM-based multiplexing scheme is essentially a particular case of the Multiple-input-Multiple-output (MIMO) system [9-10]. After some debates, the research team of Thidé acknowledged that their proposed scheme could be equivalent to the MIMO system in the case of a limited receiving aperture [11]. Guo proposed a new radar imaging scheme utilizing the electromagnetic vortex [12], and the researchers of his university did much work on the imaging model and the imaging method later on [13-15], but there are also controversies about the resolution performance of their schemes [16]. Fonseca designed a Fresnel-like reflector antenna to generate high-order orbital angular momentum states in the radio band [17]. Guan designed a new type of metasurface to generate the vortex beam of two different modes simultaneously [18]. For the scattering problem, there are only a few open literatures conducting the simulation on the OAM-based scattering of macro targets in the low-frequency radio domain [19-21], and all of these simulations are based on the ideal and analytical source model.

In this paper, we propose a modified octree grouping scheme of MLFMA [22-23] based on the method of momentum (MoM) [24-25] to conduct the approximate incorporate modeling of an electrically large scattering target and a spiral parabolic antenna efficiently. This full wave EM simulation uses a practical OAM antenna as the radiation source and takes the operating range and antenna coupling into account. Thus, it can simulate the reality as far as possible. The algorithm starts with dividing the computational region into two parts, namely radiation and scattering regions. Firstly, the induced current on the antenna (radiation region) is computed with the excitation source; secondly, the necessary radiation field is calculated as the incident field for the target (scattering region) with the induced current on the antenna, and finally the scattered field of the target (scattering region) is obtained with the

multilevel fast multipole algorithm. It should be noted that there are two octree groups built just close to the surfaces of the antenna and the target respectively, which avoids the unnecessary octree grouping of the whole solution domain in the situation of a long operating range. The simulations in this paper reveal some special scattering phenomena caused by the spiral phase distribution of the electromagnetic vortex. The near-field characteristic of the electromagnetic vortex is demonstrated by considering the effect of the operating range. We also provide further verifications and explanations for the corresponding consequences.

This paper is organized as follows. Section II describes the spatial phase distribution of the electromagnetic vortex generated by a spiral parabolic antenna with different parameter settings. Section III illustrates the modified octree grouping scheme and provides the numerical example of double metal spheres with different mode numbers. Section IV provides the numerical example of a scaled-down airplane which is illuminated by a spiral parabolic antenna at long operating ranges and some consequence analyses. Finally, further discussions and conclusions are drawn in Section V.

II. PROPAGATION OF THE ELECTROMAGNETIC VORTEX GENERATED BYA SPIRAL PARABOLIC ANTENNA

Take the spiral parabolic antenna in [6] as the example to research on the spatial phase distribution of the vortex electromagnetic beam by practical antennas. This type of OAM antennas has the advantages such as high gain, small divergence angle, high mode purity, and fits for the situation of a long operating range between the antenna and the target. Figure 1 shows the antenna model used in the following simulations. The electromagnetic vortices of different mode numbers can be achieved by means of adjusting the height of the split. Figure 2 reveals the phase distribution of the mode 1 and the mode 2 in different propagation distances through the full wave simulation. The observation planes used for sampling are perpendicular to the propagation axis Z and they are centered with the axis Z.

It can be seen that the electromagnetic vortices of nonzero modes tend to be that of the mode 0 from the beam center with the increase of the propagation distance, and the higher the mode is , the more obvious the degradation is. This is difficult to be observed with the ideal and analytical model of the electromagnetic vortex. Figure 3 shows that the spiral phase distribution can recover gradually with the expansion of the aperture.
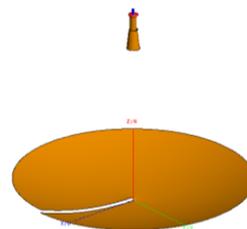
Fig. 1. The model of the spiral parabolic antenna used in numerical simulations. (The horn can be replaced by the ideal Gaussian feed source).
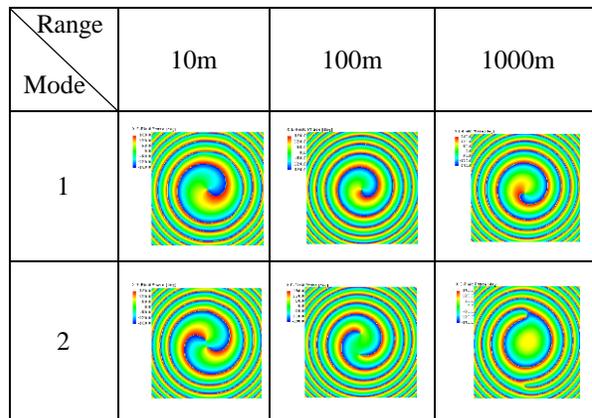
Fig. 2. The phase distribution of the electromagnetic vortex on an observation plane in different propagation distances. (The size of observation plane is 3m*3m, 10m*10m, 30m*30m from left to right; the operating frequency is 10GHz; the aperture of the parabolic antenna is 36λ, the focus length is 25λ.)
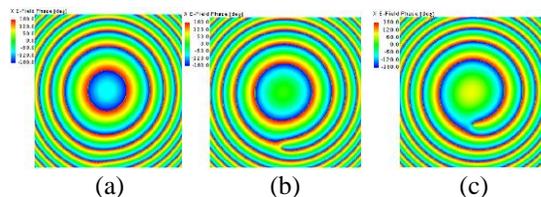
Fig. 3. The phase distribution of the mode 1 at 100km with different antenna apertures. (The aperture of the antenna is 36λ, 50λ, 80λ from (a) to (c); the size of the observation plane is 300m*300m, other parameters are same with those in Fig. 2).

As we know, the radiation pattern of the OAM beam with a nonzero mode is doughnut-like and the direction of the maximum radiation is not along the propagation axis. The phase variation along the direction of the maximum radiation is more significant. Just take the mode 1 in Fig. 2 as an example. Figure 4 (a) and Fig. 5 illustrate that the phase gradient can still be maintained along the direction of the maximum

radiation. However, this phase gradient is meaningless because the scope of the observation area is too large for common applications on radar. If the observation circle has a fixed size and it is centered with the propagation axis, the similar consequence can be obtained as Fig. 2, which is illustrated in Fig. 4 (b) and Fig. 6. The full wave simulations above show that the electromagnetic vortex by a spiral parabolic antenna has the characteristic of the near field.

(a)　　　　　　(b)
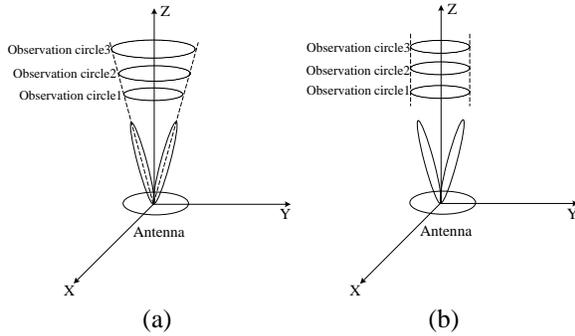
Fig. 4. Two phase sampling schemes.
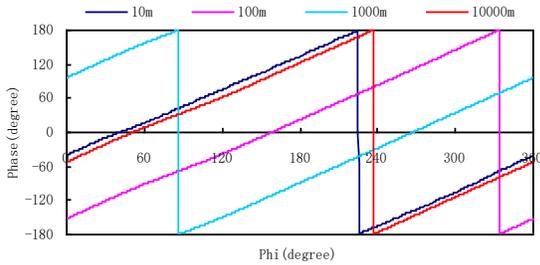
Fig. 5. The phase variation along the dynamic-sized circles which are placed along the direction of the maximum radiation.
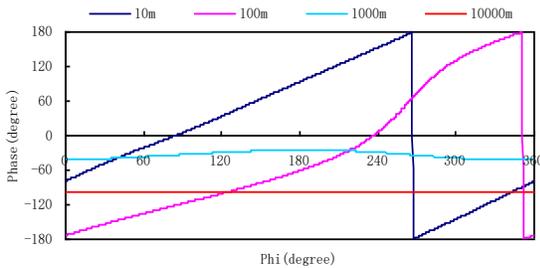
Fig. 6. The phase variation along the fix-sized circles which are placed around the propagation axis.

III. A MODIFIED OCTREE GROUPING SCHEME FOR SOLVING THE EM SCATTERING OF THE ELECTROMAGNETIC VORTEX

For analyzing the long-distance scattering problem with the method of momentum efficiently, a modified octree grouping scheme of the MLFMA is proposed and illustrated in Fig. 7. The proposed scheme divides the original incorporate solving process into three steps: the first step is to compute the induced current on the antenna with the excitation source. The induced current for a spiral parabolic antenna is computed with the electric field integrated equation (EFIE) because of the open structure:

$$\mathbf{E}_a^i(\mathbf{r})\,|_{\tan} = j\omega\mu\int\left[\mathbf{J}_a(\mathbf{r}') + \frac{1}{k^2}\nabla(\nabla'\bullet\mathbf{J}_a(\mathbf{r}'))\right]G(\mathbf{r},\mathbf{r}')d\mathbf{S}_a'\,|_{\tan}.$$

(1)

Where $\mathbf{E}_a^i$ and $\mathbf{J}_a$ denote the incident electric field and the induced current on the antenna respectively, $\mathbf{r}$ and $\mathbf{r}'$ are the observation point and the source point respectively, G is the scalar Green's function.
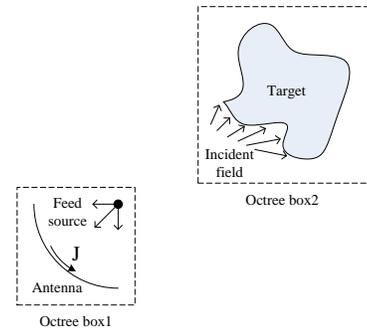
Fig. 7. The illustration of the modified octree grouping scheme for solving the electromagnetic scattering of the electromagnetic vortex generated by practical antennas.

The second step is to compute necessary radiation field (according to the location of the target) as the incident field for the target according to this induced current:

$$\mathbf{E}_t^i(\mathbf{r}) = \mathbf{E}_a^r(\mathbf{r}) = j\omega\mu\int\left[\mathbf{J}_a(\mathbf{r}') + \frac{1}{k^2}\nabla(\nabla'\bullet\mathbf{J}_a(\mathbf{r}'))\right]G(\mathbf{r},\mathbf{r}')d\mathbf{S}_a',$$

(2)

$$\mathbf{H}_t^i(\mathbf{r}) = \mathbf{H}_a^r(\mathbf{r}) = \int\mathbf{J}_a(\mathbf{r}')\times\nabla G(\mathbf{r},\mathbf{r}')d\mathbf{S}_a'.$$

(3)

Where $\mathbf{E}_a^r$ and $\mathbf{H}_a^r$ denote the radiation electric field and the radiation magnetic field of the antenna respectively, while $\mathbf{E}_t^i$ and $\mathbf{H}_t^i$ denote the incident electric field and the incident magnetic field of the target respectively

The third step is to compute the scattered field of the target by the corresponding incident field. The induced current of a close structure is computed with the combined field integrated equation (CFIE):

$$\alpha\mathbf{E}_t^i(\mathbf{r}) + (1-\alpha)\eta\mathbf{H}_t^i(\mathbf{r})\,|_{\tan} = \alpha\,j\omega\mu\int\left[\mathbf{J}_t(\mathbf{r}') + \frac{1}{k^2}\nabla(\nabla'\bullet\mathbf{J}_t(\mathbf{r}'))\right]G(\mathbf{r},\mathbf{r}')d\mathbf{S}_t'$$
$$+ (1-\alpha)\eta\int\mathbf{J}_t(\mathbf{r}')\times\nabla G(\mathbf{r},\mathbf{r}')d\mathbf{S}_t'\,|_{\tan}.$$

(4)

Where $\mathbf{J}_t$ denotes the induced current on the target, ω is the angular frequency, μ is the permeability, η is the wave impedance, and α is the combination coefficient of the CFIE from 0 to 1.

The purpose of this process is to decouple the interaction between the antenna and the target because it is weak enough to be neglected for a long operating range. The decomposition of the original incorporate solving process makes the octree group is only built close to the surfaces of the antenna and the target respectively. It avoids the unnecessary octree grouping of the whole solution domain for the incorporate modeling and the accompanying calculation cost in the situation of a long operating range. To avoid the ambiguous definition of the OAM-based RCS, we use the scattered field in the far field as the evaluation index.
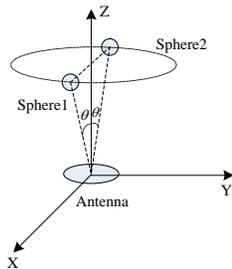
Fig. 8. Two metal spheres placed on a circle surrounding the Z-axis with an azimuthal difference of 180˚. (The solving frequency is 30GHz, the height of the spheres is 300λ and their radius is 2.5λ, they are aligned with a pitch angle of 5˚ in the XOZ plane; the aperture of the parabolic antenna is 10λ and the focus length is 15λ.)

To validate the feasibility of this approximation scheme, the bistatic scattered field of two metal spheres in the far field is shown in Fig. 8 and Fig. 9. It can be seen that well agreements between the proposed approximation method and the original incorporate modeling method by the commercial software FEKO 7.0 are achieved. The differences among the scattered field amplitudes of three modes are caused by the maximum gain of the corresponding mode as well as its direction. Drawing the curves in one chart, some special phenomena can be observed, which are shown in Fig. 10.

The variation trends of the scattered field with the pitch angle are same for the mode 0 and the mode 2, while the mode 1 is opposite. The monostatic scattered field also has the same phenomenon, as shown in Fig. 11. A similar consequence had been found by the

system experiment in [19]. This phenomenon can be explained with the distributions of the spiral phase and the target: the two metal spheres are placed on a circle surrounding the Z-axis with an azimuthal difference of 180˚, thus the phase difference between the incident fields of two spheres is 0˚ for the mode 0, 180˚ for the mode 1, and 360˚ for the mode 2 approximately. Therefore, if the scattered field for the mode 0 and the mode 2 stacks in same phase at some angles, then it is opposite for the mode 1 at these angles.

To validate this inference, we conduct another simulation furthermore, which is illustrated in Fig. 12. This time, the two metal spheres are aligned at the same height with an azimuthal difference of 90˚. It can be predicted from the inference above that the scattered field of the mode 0 and the mode 2 should have the opposite variation trend, while the mode 1 falls in between, which is proved in Fig. 13.

(a)

(b)

(c)
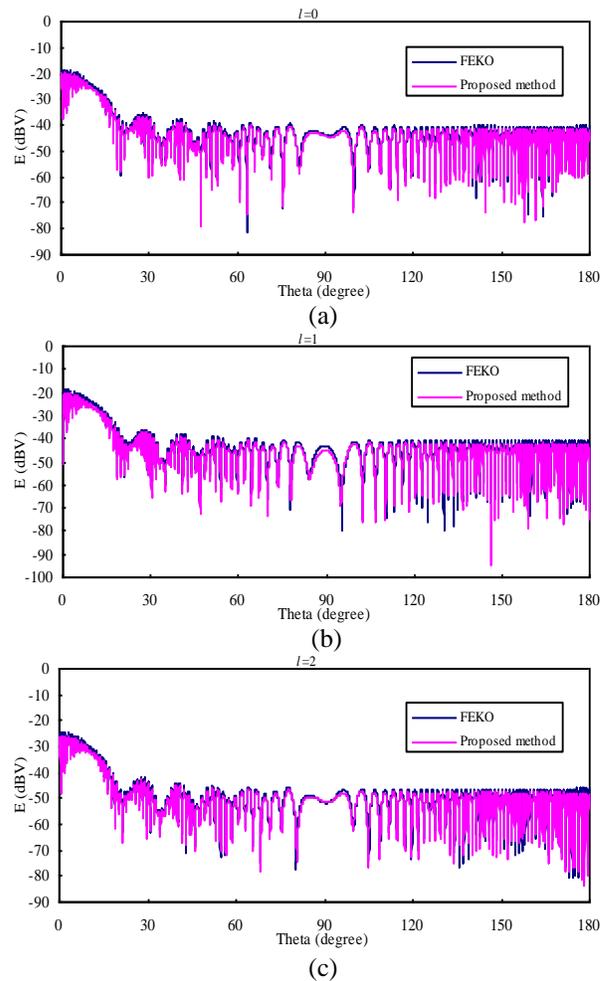
Fig. 9. The scattered electric field intensity in the far field (Phi=0˚) for the proposed method and the original method: (a) l=0, (b) l=1, and (c) l=2.
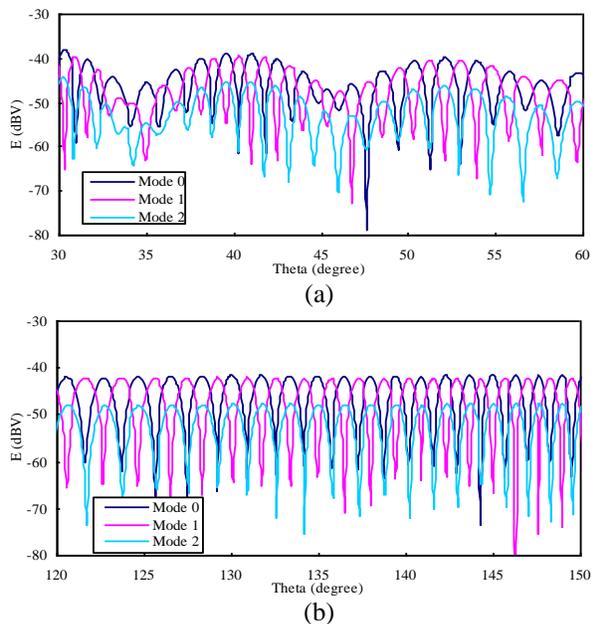
Fig. 10. The bistatic scattered field in the far field (Phi=0˚) for different mode numbers. (a) The observed pitch angle is from 30˚ to 60˚. (b) The observed pitch angle is from 120˚ to 150˚.
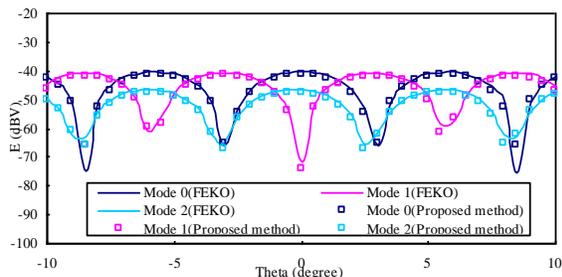
Fig. 11. The monostatic scattered field in the far field (Phi=0˚) for different mode numbers.
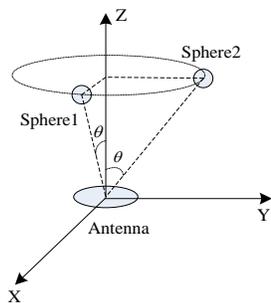
Fig. 12. Two metal spheres are placed on a circle surrounding the Z-axis with an azimuthal difference of 90˚. (Other parameters are same with those in Fig. 8).
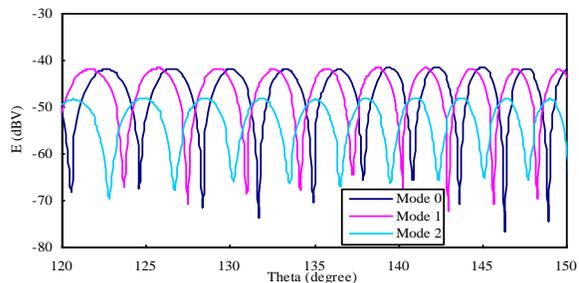
Fig. 13. The bistatic scattered field in the far field (Phi=0˚) for different mode numbers.

IV. SCATTERING OF THE ELECTROMAGNETIC VORTEX BY ELECTRICALLY LARGE TARGETS AT LONG OPERATING RANGES

To demonstrate the effect of the operating range on the scattering of the electromagnetic vortex, the bistatic scattered field of a plane model with a scaling of 0.1 compared with the real size is computed. The solving setting is illustrated in Fig. 14 and the consequences are given in Fig. 15. In this simulation, we point the direction of the maximum radiation to the nose to avoid the hollow area and the mode degradation. Meanwhile, the mode 10 in Fig. 15 is generated by a modified spiral parabolic antenna proposed in [17] to ensure its purity.
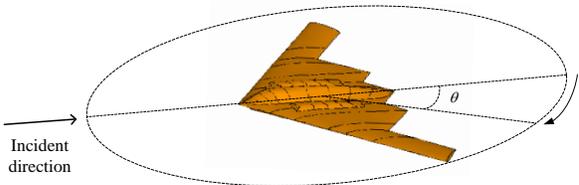
Fig. 14. The bistatic scattering computation of a scaled-down plane model.

It can be seen from Fig. 15 that with the increase of the operating range, the variation trends of the scattered field tend to be the same as the mode 0, and the lower the mode is, the more obvious this phenomenon is. It also can be explained by the phase distribution in the far field.

As shown in Fig. 16, when the target is placed along the direction of the maximum radiation, the azimuthal variation for the target becomes smaller and smaller with the increase of the distance. It means the phase gradient of the incident field is unapparent and the incident field can be approximated to the plane wave locally just as the mode 0. Therefore, there is a pair of contradictions for the practical OAM-based radar application because of this special beam structure:

the null region of the vortex electromagnetic beam can't be used for the detection, while the direction of the annular beam can't reflect the phase gradient of the electromagnetic vortex for a size-limited target. These lead to the limited usage of the OAM in the radar realm, which is eager to be solved in the future research.
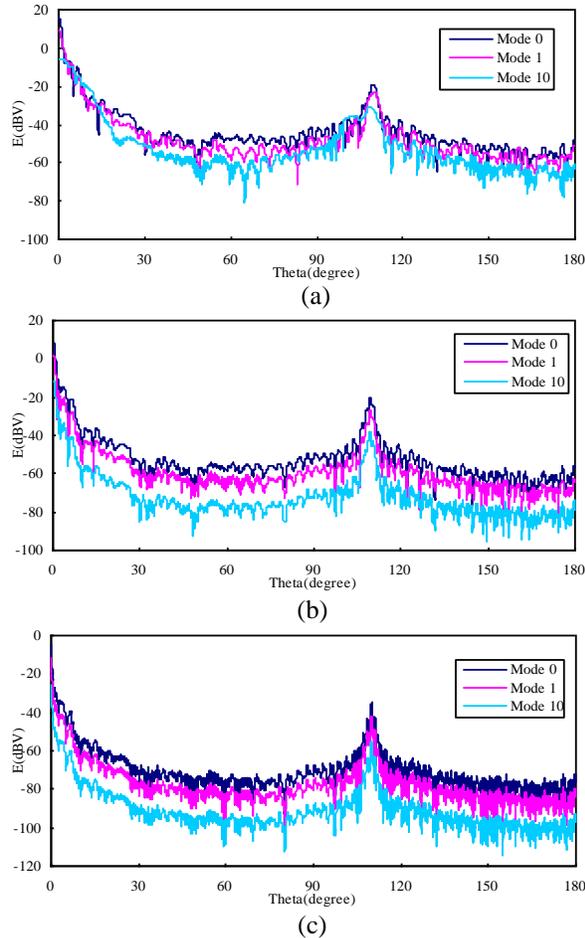
Fig. 15. The bistatic scattered field in the far field of the plane model; (a), (b) and (c) are corresponding to the operating range of 10m, 100m and 1000m respectively.
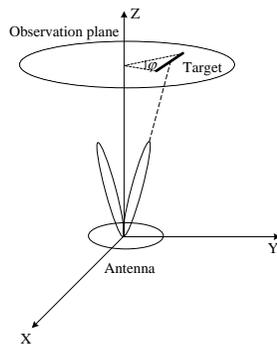
Fig. 16. The positional relationship between the antenna and the target in the far field.

V. CONCLUSION

To summarize, the approximate incorporate modeling of an electrically large scattering target and a practical antenna is conducted in this paper. The octree grouping scheme is modified to solve the EM scattering problem based on the electromagnetic vortex. The phase distributions of the field near the propagation axis in different propagation distances are simulated, which prove the degradation characteristic for the vortex electromagnetic beam generated by a spiral parabolic antenna. The numerical simulation of an airplane model and a spiral parabolic antenna reveals a pair of contradictions for the OAM-based radar application. However, during its effective operating range, the scattered field may show a regular difference compared to the plane wave for some particular structures. This research demonstrates the significant effect of the operating range for the OAM-based radar application in the real world. The following work includes narrowing the divergence angle of the electromagnetic vortex, generating the electromagnetic vortex with very high modes, and exploring some suitable applications during appropriate operating ranges.

ACKNOWLEDGMENT

REFERENCES

[1] L. Allen, M. W. Beijersbergen, R. J. C. Spreeuw, *et al.*, "Orbital angular momentum of light and transformation of Laguerre Gaussian laser modes," *Physical Review A*, vol. 45, no. 11, pp. 8185-8189, 1992.

[2] M. Yang, Y. Wu, K. F. Ren, and X. Sheng, "Computation of radiation pressure force exerted on arbitrary shaped homogeneous particles by high-order Bessel vortex beams using MLFMA," *Optics Express*, vol. 24, no. 24, p. 27979, 2016.

[3] M. Krenn, J. Handsteiner, M. Fink, *et al.*, "Twisted light transmission over 143 kilometers," *Proceedings of the National Academy of Sciences*, 2016.

[4] M. P. J. Lavery, F. C. Speirits, S. M. Barnett, *et al.*, "Detection of a spinning object using light's orbital angular momentum," *Science*, vol. 341, no. 6145, pp. 537-540, 2013.

[5] B. Thidé, H. Then, J. SjÖHolm, *et al.*, "Utilization of photon orbital angular momentum in the low-frequency radio domain," *Physical Review Letters*, vol. 99, no. 8, p. 087701, 2007.

[6] F. Tamburini, E. Mari, A. S Ponselli, *et al.*,

"Encoding many channels in the same frequency through radio vorticity: first experimental test," *New Journal of Physics*, vol. 14, no. 11, pp. 78001-78004, 2011.

[7] F. Tamburini, E. Mari, B. Thidé, *et al*., "Experimental verification of photon angular momentum and vorticity with radio techniques," *Applied Physics Letters*, vol. 99, no. 20, p. 204102, 2011.

[8] F. Tamburini, B. Thidé, V. Boaga, *et al*., "Experimental demonstration of free-space information transfer using phase modulated orbital angular momentum radio," *Physics*, 2013.

[9] O. Edfors and A. J. Johansson, "Is orbital angular Momentum (OAM) Based Radio Communication an unexploited area," *IEEE Transactions on Antennas and Propagation*, vol. 60, no. 2, pp. 1126-1131, 2012.

[10] M. Tamagnone, C. Craeye, and J. Perruisseau-Carrier, "Comment on 'encoding many channels on the same frequency through radio vorticity: First experimental test'," *New Journal of Physics*, vol. 14, no. 11, p. 118001, 2012.

[11] M. Oldoni, F. Spinello, E. Mari, *et al*., "Space-division demultiplexing in orbital-angular-momentum based MIMO radio systems," *IEEE Transactions on Antennas and Propagation*, vol. 63, no. 10, pp. 1-1, 2015.

[12] G. R. Guo, W. D. Hu, and X. Y Du, "Electromagnetic vortex based radar target imaging," (in Chinese) *Journal of National University of Defense Technolology*, vol. 35, no. 6, pp. 71-76, Dec. 2013.

[13] K. Liu, Y. Q. Cheng, Z. C. Yang, *et al*., "Orbital-angular-momentum-based electromagnetic vortex imaging," *IEEE Antennas and Wireless Propagation Letters*, vol. 14, pp. 711-714, 2015.

[14] T. Z. Yuan, H. Q. Wang, Y. L. Qin, *et al*., "Electromagnetic vortex imaging using uniform concentric circular arrays," *IEEE Antennas and Wireless Propagation Letters*, vol. 15, pp. 1-1, 2015.

[15] K. Liu, Y. Q. Cheng, Y. Gao, *et al*., "Super-resolution radar imaging based on experimental OAM beams," *Applied Physics Letters*, vol. 110, no. 16, p. 164102, 2017.

[16] B. Tang, K. Y. Guo, J. P. Wang, *et al*., "Resolution performance of the orbital-angular-momentum-based imaging radar," *IEEE Antennas and Wireless Propagation Letters*, vol. 16, pp. 2975-2978, 2017.

[17] N. J. G. Fonseca, L. Coulomb, and J. C. Angevain, "A Fresnel-like reflector antenna design for high-order orbital angular momentum states," *IEEE European Conference on Antennas & Propagation*, 2015.

[18] L. Guan, Z. He, D. Z. Ding, Y. F. Yu, W. Zhang and R. S. Chen, "Polarization-controlled shared-aperture metasurface for generating the vortex beam with different modes," *IEEE Transactions on Antennas and Propagation*, vol. 66, no. 12, pp. 7455-7459, Dec. 2018.

[19] C. Zhang, D. Chen, and X. Jiang, "RCS diversity of electromagnetic wave carrying orbital angular momentum," *Scientific Reports*, vol. 7, no. 1, p. 15412, 2017.

[20] M. P. Yu, Y. P. Han, and Z. W. Cui, "Scattering of non-diffracting vortex electromagnetic wave by typical targets," *Progress In Electromagnetics Research Letters*, vol. 70, pp. 139-146, 2017.

[21] K. Liu, Y. Gao, X. Li, *et al*., "Target scattering characteristics for OAM-based radar," Aip Advances, vol. 8, no. 2, p. 025002, 2018.

[22] Z. He, H. H. Zhang, and R. S. Chen, "Parallel marching-on-in-degree solver of time-domain combined field integral equation for bodies of revolution accelerated by MLACA," *IEEE Transactions on Antennas and Propagation*, vol. 63, no. 8, pp. 3705-3710, Aug. 2015.

[23] J. H. Gu, Z. H. Fan, D. Z. Ding, and R. S. Chen, "A low frequency EFIE-MLFMA solver based on approximate diagonalization of the green's function," *IEEE Transactions on Antennas and Propagation*, vol. 65, no. 12, pp. 7150-7156, Dec. 2017.

[24] Z. He, J. H. Gu, W. Sha, and R. S. Chen, "An efficient volumetric method of moments for modeling plasmonic thin-film solar cells with periodic structures," *Optics Express*, vol. 26, no. 19, pp. 25037-25046, Nov. 2018.

[25] K. C. Wang, Z. He, D. Z. Ding, and R. S. Chen, "Uncertainty scattering analysis of 3-D objects with varying shape based on method of moments," *IEEE Transactions on Antennas and Propagation*, vol. 67, no. 4, pp. 2835-2840, Apr. 2019.

Bihuan Yin was born in Jiangsu, China. He received the B.Sc. degree in Communication Engineering from the School of Electrical Engineering and Optical Technique, Nanjing University of Science and Technology, Nanjing, China, in 2014, where he is currently working towards the Ph.D. degree.

His research interests include computational electromagnetics, radar imaging, and orbital angular momentum.

Zi He was born in Hebei, China. She received the B.Sc. and Ph.D. degrees in Electronic Information Engineering from the School of Electrical Engineering and Optical Technique, Nanjing University of Science and Technology, Nanjing, China, in 2011 and 2016, respectively. She has worked as a visiting scholar in the University of Illinois at Urbana and Champaign (UIUC) from September 2015 to September 2016. She works as a postdoctor at the Science and Technology on Electromagnetic Scattering Laboratory, BIEF.

Since 2016, she has been an Assistant Professor with the Department of Communication Engineering, Nanjing University of Science and Technology. Her research interests include antenna, RF-integrated circuits, and computational electromagnetics.

Rushan Chen was born in Jiangsu, China. He received the B.Sc. and M.Sc. degrees from the Department of Radio Engineering, Southeast University, China, in 1987 and 1990, respectively, and the Ph.D. degree from the Department of Electronic Engineering, City University of Hong Kong, in 2001.

He joined the Department of Electrical Engineering, Nanjing University of Science and Technology (NJUST), China, where he became a Teaching Assistant in 1990 and a Lecturer in 1992. Since September 1996, he has been a Visiting Scholar with the Department of Electronic Engineering, City University of Hong Kong, first as Research Associate, then as a Senior Research Associate in July 1997, a Research Fellow in April 1998, and a Senior Research Fellow in 1999. From June to September 1999, he was also a Visiting Scholar at Montreal University, Canada. In September 1999, he was promoted to Full Professor and Associate Director of the Microwave and Communication Research Center in NJUST, and in 2007, he was appointed as the Head of the Department of Communication Engineering, NJUST. He was appointed as the Dean in the School of Communication and Information Engineering, Nanjing Post and Communications University in 2009. And in 2011 he was appointed as Vice Dean of the School of Electrical Engineering and Optical Technique, NJUST. Currently, he is a principal investigator of more than 10 national projects. His research interests mainly include computational electromagnetics, microwave integrated circuit and nonlinear theory, smart antenna in communications and radar engineering, microwave material and measurement, RF-integrated circuits, etc. He has authored or coauthored more than 260 papers, including over 180 papers in international journals.